



HAL
open science

CaCu₃Ti₄O₁₂, an efficient catalyst for ibuprofen removal by activation of peroxymonosulfate under visible-light irradiation

Yunqing Zhu, Tian Wang, Wenjuan Wang, Siyu Chen, Eric Lichtfouse, Cheng Cheng, Jie Zhao, Yingxuan Li, Chuanyi Wang

► **To cite this version:**

Yunqing Zhu, Tian Wang, Wenjuan Wang, Siyu Chen, Eric Lichtfouse, et al.. CaCu₃Ti₄O₁₂, an efficient catalyst for ibuprofen removal by activation of peroxymonosulfate under visible-light irradiation. *Environmental Chemistry Letters*, 2019, 17 (1), pp.481-486. 10.1007/s10311-018-0776-x . hal-02082946

HAL Id: hal-02082946

<https://hal.science/hal-02082946>

Submitted on 28 Mar 2019

HAL is a multi-disciplinary open access archive for the deposit and dissemination of scientific research documents, whether they are published or not. The documents may come from teaching and research institutions in France or abroad, or from public or private research centers.

L'archive ouverte pluridisciplinaire **HAL**, est destinée au dépôt et à la diffusion de documents scientifiques de niveau recherche, publiés ou non, émanant des établissements d'enseignement et de recherche français ou étrangers, des laboratoires publics ou privés.

CaCu₃Ti₄O₁₂, an efficient catalyst for ibuprofen removal by activation of peroxymonosulfate under visible-light irradiation

Yunqing Zhu^{1,2} · Tian Wang¹ · Wenjuan Wang¹ · Siyu Chen³ · Eric Lichtfouse⁴ · Cheng Cheng¹ · Jie Zhao¹ · Yingxuan Li¹ · Chuanyi Wang¹

Abstract

Contamination of waters by pharmaceuticals is a major health issue. Therefore, there is a need for efficient techniques to remove pharmaceutical pollutants. Here, a photo-assisted fenton-like method based on sulfate radicals was tested using CaCu₃Ti₄O₁₂ with different morphologies as catalyst. Sintering of CaCu₃Ti₄O₁₂ at 775 °C for 6 h produced cubic structures with sizes from 2 to 5 μm, whereas sintering for 14 h produced microfibers, according to scanning electron microscopy. The highest electron paramagnetic resonance signal was observed for 6-h sintering. We evaluated the catalytic efficiency of CaCu₃Ti₄O₁₂ for ibuprofen degradation with peroxymonosulfate under visible light. Results show that CaCu₃Ti₄O₁₂ and 0.5 mM peroxymonosulfate under visible-light irradiation induced 91.8% removal of ibuprofen in 60 min. The Cu⁺ vacancy on the surface of CaCu₃Ti₄O₁₂ is essential to activate the sulfate radicals by forming a Cu⁺–Cu²⁺ redox couple, which led to the rapid and efficient removal of ibuprofen.

Keywords Advanced oxidation · CaCu₃Ti₄O₁₂ · Peroxymonosulfate · Photocatalysis · Ibuprofen

Introduction

In recent years, the Fenton-like process based on the sulfate radical SO₄^{•-} (Luo et al. 2017; Zhu et al. 2013) has attracted increasing interest as an alternative to the traditional Fe²⁺/

H₂O₂ process with active species of hydroxyl radicals for treating recalcitrant organic pollutants. Indeed, SO₄^{•-}, with a higher oxidative potential (2.5–3.1 V), displays a higher oxidation power compared to ·OH (Lian et al. 2017). In addition, SO₄^{•-} also has a wide pH operating range, from 2 to 9, and long half-life time of 30–40 μs (Ding et al. 2016), which is expected to be more efficient performance in environmental remediation. However, the generation of SO₄^{•-} from peroxydisulfate and peroxymonosulfate under normal conditions is generally slow. Recently, activating peroxydisulfate or peroxymonosulfate with UV irradiation (Huang et al. 2017), transition metal ions (like Co²⁺, Cu²⁺ or Fe²⁺) (Bu et al. 2016; Zou et al. 2014) and metal oxides (Fang et al. 2017; Gong et al. 2015) has been tested to accelerate the reaction. It was found that the metal catalysts employed to activate peroxymonosulfate have exhibited reliable performance for the treatment of organic pollutants. Among those catalysts, Co₃O₄ was frequently studied due to its high efficiency in peroxymonosulfate activation.

More recently, photocatalytic activation of peroxymonosulfate for contaminants removal under visible light has attracted plenty of attention (Fernandez et al. 2004; Yang et al. 2008; Yi et al. 2017). The removal efficiency is enhanced by coupling peroxymonosulfate with

Electronic supplementary material The online version of this article (<https://doi.org/10.1007/s10311-018-0776-x>) contains supplementary material, which is available to authorized users.

✉ Yunqing Zhu
zhuyunqing@sust.edu.cn

✉ Eric Lichtfouse
eric.lichtfouse@inra.fr

✉ Chuanyi Wang
wangchuanyi@sust.edu.cn

¹ School of Environmental Science and Engineering, Shaanxi University of Science and Technology, Xi'an 710021, China

² Zhejiang Wenzhou Research Institute of Light Industry, Wenzhou 325804, China

³ School of Chemistry and Chemical Engineering, Shihezi University, Shihezi 823000, China

⁴ Aix-Marseille Univ, CEREGE, Coll de France, CNRS, INRA, IRD, Avenue Louis Philibert, 13545 Aix en Provence, France

photocatalysts, as a result of (1) electron trapping, which reduces the recombination of electrons and holes (Jaafarzadeh et al. 2017) and (2) generation of SO_4^- radicals (Ghanbaria et al. 2016). Chen et al. (2012) have tested the use of TiO_2 -peroxymonosulfate under visible-light irradiation. Wang's group has found that one-dimensional (1D) Co_3O_4 nanorods showed a high catalytic activity for phenol oxidation with sulfate radicals under visible-light irradiation (Wang et al. 2015). Liu et al. (2016a, b) demonstrated that in the presence of peroxymonosulfate, the photocatalytic efficiency of BiVO_4 and the removal rate of Rhodamine B can be enhanced by sulfate radicals, hydroxyl radicals and superoxide radicals. In addition, S-TiO_2 (Jiang et al. 2017), C_3N_4 (Khan et al. 2017) and manganese oxide molecular sieves (Duan et al. 2015) were also investigated for contaminants removal under visible light coupled with peroxymonosulfate. However, the development of efficient and stable catalysts for the generation of SO_4^- is still highly desired, which is one of the most important factors affecting the efficiency of peroxymonosulfate-photocatalysis system.

$\text{CaCu}_3\text{Ti}_4\text{O}_{12}$ is a kind of ABO_3 perovskite, which has been intensively studied due to its very high dielectric constant (Ponce et al. 2015; Luo et al. 2015; Zhang et al. 2016). Moreover, recent studies indicate that the $\text{CaCu}_3\text{Ti}_4\text{O}_{12}$ material displays visible-light-induced photocatalytic activity (Clark et al. 2011; Kushwaha et al. 2016). It is recognized that the Cu-based occupied states in $\text{CaCu}_3\text{Ti}_4\text{O}_{12}$ are higher in energy than the O2p-based valence band, which trigger the visible-light-induced photocatalytic activity (Clark et al. 2011). The visible-light-induced charges, transferring from Cu^{2+} and Ti^{4+} ground state to Cu^{3+} and Ti^{3+} excited state, are free to move in the distinct ordered crystallographic sub-lattices, and thereby involved in the photocatalytic reaction. In addition, the photo-generated free electrons can relax into the localized Cu 3d band within band gap to form Cu^+ , and the excitation of electrons from valence band makes also possible to their migration to the localized Cu 3d-O 2p band thus accelerating the generation of Cu^+ . Based on the previous studies (Lei et al. 2015), it was thought that the formed $\text{Cu}^+ - \text{Cu}^{2+}$ and $\text{Cu}^{2+} - \text{Cu}^{3+}$ redox pairs are beneficial to facilitating the activation of peroxymonosulfate to generated SO_4^- . However, the photocatalytic activation of peroxymonosulfate with $\text{CaCu}_3\text{Ti}_4\text{O}_{12}$ has been barely studied till now.

Here, the photocatalytic removal of ibuprofen using $\text{CaCu}_3\text{Ti}_4\text{O}_{12}$ with peroxymonosulfate under visible-light irradiation has been explored for the first time. Cubic and fiber-shaped $\text{CaCu}_3\text{Ti}_4\text{O}_{12}$ catalysts were prepared via a molten salt method. The removal efficiency of ibuprofen was tested, and the reaction mechanism was also discussed.

Materials and methods

Preparation and characterization of $\text{CaCu}_3\text{Ti}_4\text{O}_{12}$

$\text{CaCu}_3\text{Ti}_4\text{O}_{12}$ (CCTO) powders were prepared by a molten salt process. Typically, stoichiometric amounts of TiO_2 (Aldrich, 99.9%), CuO (Aldrich, 99.9%) and CaO (Aldrich, 99.99%) were mixed with the mixed salts of NaCl and KCl ($\text{NaCl}:\text{KCl}=1:1$) with salt/precursor ratio of 3.55, and then, the mixture was ball-milled in alcohol for 8 h in order to obtain a homogeneous mixture with reduced particle size. After alcohol evaporation, the resulting powder was transferred into a corundum crucible and sintered at 775°C in a muffle furnace with heating rate of $10^\circ\text{C}/\text{min}$ in air for 6, 10, 14, 18 h. The obtained $\text{CaCu}_3\text{Ti}_4\text{O}_{12}$ powder was washed with pure water for several times and grinded to reduce particle size and labeled as CCTO-6, CCTO-10, CCTO-14, CCTO-18 according to the sintering time 6, 10, 14, 18 h, respectively. The as-prepared $\text{CaCu}_3\text{Ti}_4\text{O}_{12}$ samples were examined by scanning electron microscope (SEM), X-ray diffraction (XRD), electron paramagnetic resonance (EPR) and the X-ray photoelectron spectroscopy (XPS).

Catalytic removal experiment

Ibuprofen was used as a target pollutant to evaluate the catalytic removal efficiency of $\text{CaCu}_3\text{Ti}_4\text{O}_{12}$ with peroxymonosulfate under visible-light irradiation. Typically, $\text{CaCu}_3\text{Ti}_4\text{O}_{12}$ was added to 100 mL ibuprofen solution (20 mg L^{-1}), and the suspension was adjusted to neutral pH. The suspensions were vigorously stirred in the dark for 30 min, and then, Oxone (KHSO_5 as active component, Aldrich) was added into the solution at $\text{KHSO}_5/\text{ibuprofen}$ molar ratio of 5:1. Then, the suspensions were irradiated by 300 W xenon lamp equipped with a UV cutoff filter ($\lambda \geq 420\text{ nm}$) at room temperature. Two milliliters of solution was taken out at a given time interval for analysis of ibuprofen concentration. Ibuprofen concentrations were determined by Thermo Fisher Ultra 3000 HPLC equipped with a $25\text{ cm} \times 4.6\text{ mm}$ Cosmosil C18 column.

Results and discussion

Microscopic characterization of $\text{CaCu}_3\text{Ti}_4\text{O}_{12}$

Figure 1 shows the scanning electron microscope (SEM) images of the synthesized $\text{CaCu}_3\text{Ti}_4\text{O}_{12}$ (CCTO) samples. Results show that the $\text{CaCu}_3\text{Ti}_4\text{O}_{12}$ samples display very different morphology by sintering at 775°C for different time. The CCTO-6 sintered at 775°C for 6 h (Fig. 1a) displays

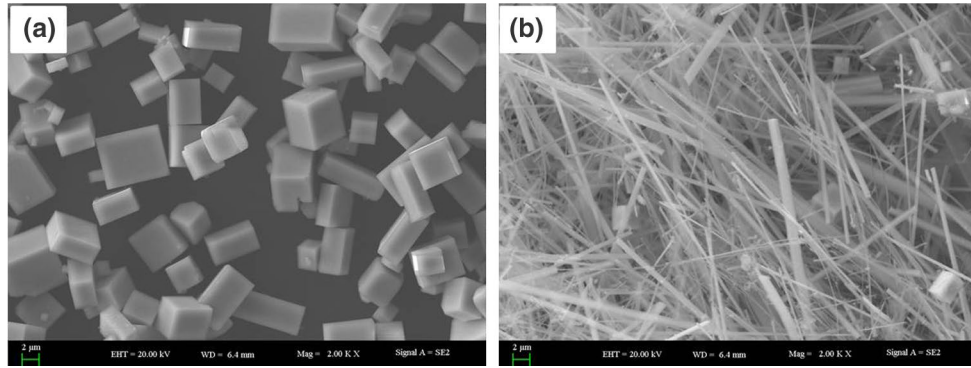


Fig. 1 Scanning electron microscope (SEM) images of $\text{CaCu}_3\text{Ti}_4\text{O}_{12}$ (CCTO) samples sintering at different times: **a** 6-h sintering; **b** 14-h sintering. The CCTO-6, sintered at 775 °C for 6 h, displays cubic structures with 2–5 μm sizes. The CCTO-14 sample, sintered

for 14 h, exhibits a microfiber structure. Only small amounts of $\text{CaCu}_3\text{Ti}_4\text{O}_{12}$ particles still retain the cubic structure and the size is further decreased

a cubic structure with size from 2 to 5 μm . Increasing the heat-treating time to 10 h, the majority of CCTO-10 samples still kept cubic morphology, but became irregular, and the size was reduced to less than 2 μm . The edge of the cubic CCTO-10 samples was become rough in comparison with CCTO-6, and other new facets were formed. More important, the micro-sized CCTO fibers were formed with about several hundred nanometer in diameter and tens micrometer in length. Further increasing the sintering time to 14 h, as shown in Fig. 1b, induces the majority of the CCTO-14 samples to exhibit a microfiber structure. Only a small amount of $\text{CaCu}_3\text{Ti}_4\text{O}_{12}$ particles still retains the cubic structure, and the size is further decreased. The remaining cubic $\text{CaCu}_3\text{Ti}_4\text{O}_{12}$ particles are distributed randomly in the microfibers. Further, with the sintering time increasing to 18 h, only $\text{CaCu}_3\text{Ti}_4\text{O}_{12}$ microfibers are observed, and the cubic structures of $\text{CaCu}_3\text{Ti}_4\text{O}_{12}$ are hardly found. The diameter of CCTO-18 sample is about a hundred nanometer and the length is increased to about 100 μm .

Structural characterization of $\text{CaCu}_3\text{Ti}_4\text{O}_{12}$

Figure 2a shows the XRD patterns of synthesized $\text{CaCu}_3\text{Ti}_4\text{O}_{12}$ powders. By heat treating at 775 °C for different time periods, the obtained $\text{CaCu}_3\text{Ti}_4\text{O}_{12}$ samples display cubic crystal structure according to standard JCPDS card (number: 75–2188) of pure $\text{CaCu}_3\text{Ti}_4\text{O}_{12}$. And from Fig. 2a, it is also observed that the samples display a trace of secondary phases of CuO and TiO_2 . However, with the increasing of sintering time, the peak intensity of CuO, and TiO_2 secondary phases is reduced, indicating that the amount of impurity phases is decreased. Additionally, the intensity ratio between (400) facet at 49.4° and (422) facet at 61.5° is different with the increasing of heat-treating time, which maybe ascribe to the morphology evolution from cubic to fiber. The Raman spectroscopy was also

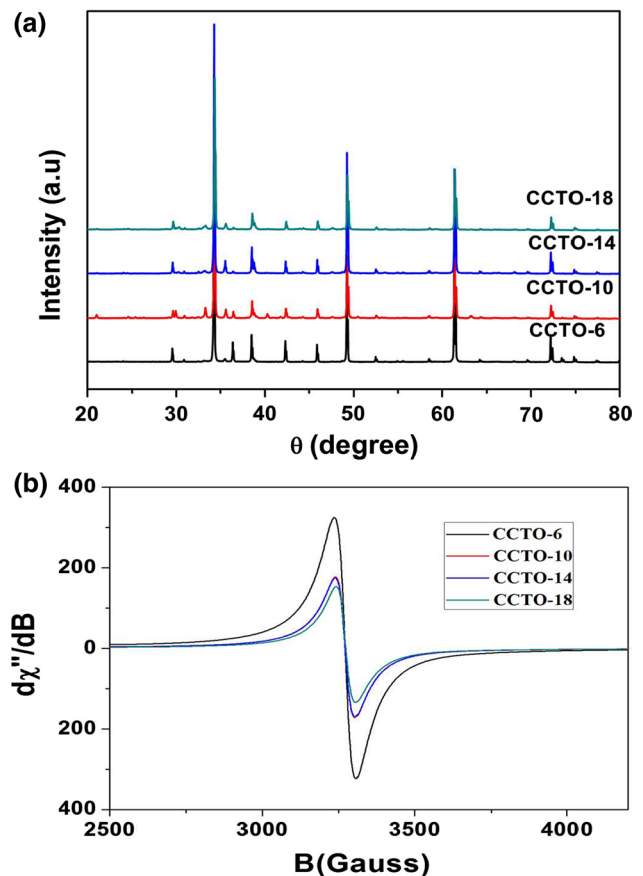


Fig. 2 a X-ray diffraction (XRD) patterns of $\text{CaCu}_3\text{Ti}_4\text{O}_{12}$ (CCTO) samples. Only the cubic crystal structure of pure $\text{CaCu}_3\text{Ti}_4\text{O}_{12}$ was observed; JCPDS number: 75–2188. **b** Electron paramagnetic resonance (EPR) spectra of $\text{CaCu}_3\text{Ti}_4\text{O}_{12}$ samples. EPR lines of all $\text{CaCu}_3\text{Ti}_4\text{O}_{12}$ samples are ideally fitted by the Lorentzian line with a linewidth (ΔH_{pp}) of 7.1 mT. CCTO-6, sintered at 775 °C for 6 h, displayed the highest EPR signal intensity among the four $\text{CaCu}_3\text{Ti}_4\text{O}_{12}$ samples (6, 10, 14 and 18 h), as the intensity of the EPR signal decreased with heat-treating time. *a.u.* arbitrary units

performed to identify the crystal structure of $\text{CaCu}_3\text{Ti}_4\text{O}_{12}$. For sample CCTO-6, a broadband around $400\text{--}500\text{ cm}^{-1}$ is observed, and with the increase in sintering time to 14 h, the intensity of the broadband is enhanced. This behavior is in good agreement with the XRD results. However, for the sample sintered for 18 h, the Raman peaks are separated to two peaks at 445 and 508 cm^{-1} . This mode in the CCTO-18 sample is normal Raman-active in good agreement with values reported in the literature (Almeida et al. 2002; Ramirez et al. 2000). The peaks at 445 and 508 cm^{-1} are associated with the A_g symmetry (TiO_6 rotation like) modes.

Figure 2b shows the electron paramagnetic resonance (EPR) spectrum for the $\text{CaCu}_3\text{Ti}_4\text{O}_{12}$ samples at 294 K. A unique broad and symmetric signal for the $\text{CaCu}_3\text{Ti}_4\text{O}_{12}$ centered around $g \sim 2.06$ is observed, which comes from the Cu^{2+} paramagnetic center (Vivas et al. 2017). The EPR lines of all the $\text{CaCu}_3\text{Ti}_4\text{O}_{12}$ samples are ideally fitted by the Lorentzian line with a linewidth (ΔH_{pp}) of 7.1 mT. As shown in Fig. 2b, the signal intensity decreases with the increase in heat-treating time, indicating that in the molten salt process, the heat treating can promote the generation of oxygen vacancies, which further producing the reduction of Cu^{2+} to Cu^+ . The transfer from Cu^{2+} to Cu^+ leads to the decrease in EPR signal intensity due to the poor contribution of Cu^+ to the EPR spectrum (Luo et al. 2015). The XPS spectra (Fig. S2) also prove the presence of Cu^+ in the $\text{CaCu}_3\text{Ti}_4\text{O}_{12}$ samples. The presence of Cu^+ and Cu^{2+} couple will participate in the activation of peroxymonosulfate for the generation of sulfur radicals.

Catalytic activity and stability of $\text{CaCu}_3\text{Ti}_4\text{O}_{12}$

The removal of ibuprofen was carried out in various systems for testing the photo-assisted activation of peroxymonosulfate with $\text{CaCu}_3\text{Ti}_4\text{O}_{12}$. After 30 minutes adsorption equilibrium, the CCTO performs negligible adsorption capability for ibuprofen. First, the removal of ibuprofen in the binary system of visible light/ $\text{CaCu}_3\text{Ti}_4\text{O}_{12}$, visible light/peroxymonosulfate, $\text{CaCu}_3\text{Ti}_4\text{O}_{12}$ /peroxymonosulfate, and ternary system of visible light/ $\text{CaCu}_3\text{Ti}_4\text{O}_{12}$ /peroxymonosulfate was compared. As shown in Fig. 3a, the visible-light/peroxymonosulfate and visible-light/ $\text{CaCu}_3\text{Ti}_4\text{O}_{12}$ systems performed low efficiency in ibuprofen removal, and only 3.0% (visible light/peroxymonosulfate) and 8.1% (visible light/ $\text{CaCu}_3\text{Ti}_4\text{O}_{12}$) of ibuprofen were degraded in 60 min, implying that the activation of peroxymonosulfate under visible light and the visible-light-induced photocatalytic activity of $\text{CaCu}_3\text{Ti}_4\text{O}_{12}$ possess low efficiency. The $\text{CaCu}_3\text{Ti}_4\text{O}_{12}$ /peroxymonosulfate system with peroxymonosulfate concentration of 0.5 mmol L^{-1} induced 35.5% removal of ibuprofen in 60 min (Fig. 3a).

Compared to the above binary systems, our results show that the ternary system of visible light/ $\text{CaCu}_3\text{Ti}_4\text{O}_{12}$ /

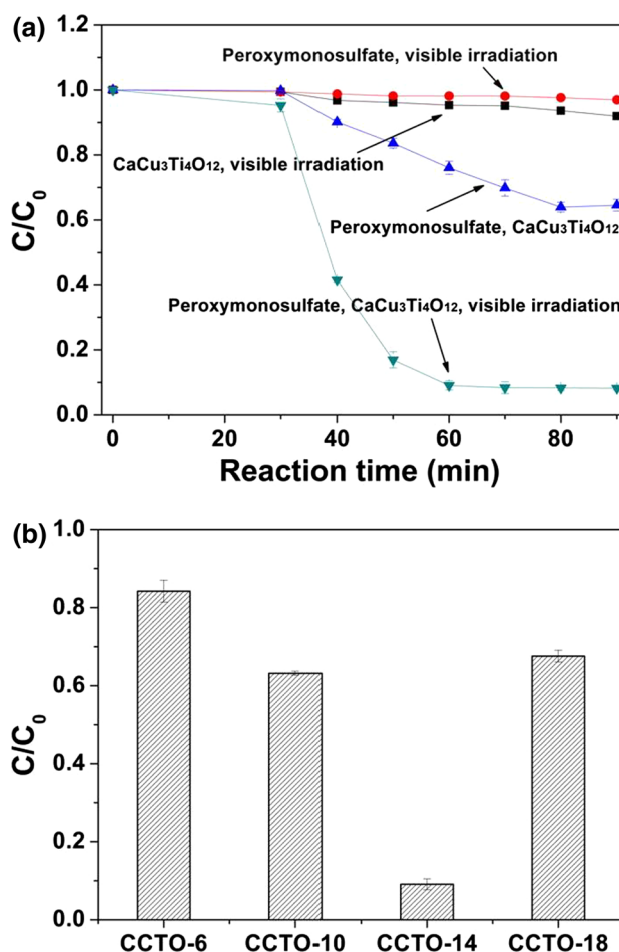


Fig. 3 a Comparison of ibuprofen removal for the systems: visible light/ $\text{CaCu}_3\text{Ti}_4\text{O}_{12}$ (CCTO), visible light/peroxymonosulfate, $\text{CaCu}_3\text{Ti}_4\text{O}_{12}$ /peroxymonosulfate, and visible light/ $\text{CaCu}_3\text{Ti}_4\text{O}_{12}$ /peroxymonosulfate. Only 3.0% of ibuprofen removal was achieved using the visible-light/peroxymonosulfate system, and 8.1% for the visible-light/ $\text{CaCu}_3\text{Ti}_4\text{O}_{12}$ system. But for the $\text{CaCu}_3\text{Ti}_4\text{O}_{12}$ /peroxymonosulfate system, ibuprofen removal increased to 35.5% in 90 min, and further increases to 91.8% at 60 min for visible-light/ $\text{CaCu}_3\text{Ti}_4\text{O}_{12}$ /peroxymonosulfate system with a peroxymonosulfate concentration of 0.5 mmol L^{-1} . b Ibuprofen removal with different $\text{CaCu}_3\text{Ti}_4\text{O}_{12}$ catalysts with visible-light/ $\text{CaCu}_3\text{Ti}_4\text{O}_{12}$ /peroxymonosulfate system in 30-min reaction. CCTO-14, calcinated for 14 h, displayed 91.0% removal of ibuprofen and the other samples exhibited relatively low removal efficiency

peroxymonosulfate in the presence of 0.5 mM peroxymonosulfate promotes the removal of ibuprofen to 91.8% in 60 min. The comparison of $\text{CaCu}_3\text{Ti}_4\text{O}_{12}$ samples at different sintering times in salt-melt process was also performed. Figure 3b shows that the CCTO-14 (calcinated for 14 h) displayed higher efficiency in ibuprofen removal (90% in 30 min) and the other samples exhibited relatively low removal efficiency (about 37%) in the visible light/ $\text{CaCu}_3\text{Ti}_4\text{O}_{12}$ /peroxymonosulfate. The presence of Cu^+ in the $\text{CaCu}_3\text{Ti}_4\text{O}_{12}$ lattice was thought to act as the active sites

for peroxymonosulfate activation (Ding et al. 2016) and dominated the removal of ibuprofen. The XPS was performed to further prove the presence of Cu^+ vacancy in the $\text{CaCu}_3\text{Ti}_4\text{O}_{12}$ lattice. As shown in Fig. 4a, the copper was present as copper oxide with $2\text{P}_{3/2}$ peak at 933.6 eV and $2\text{P}_{1/2}$ peak at 953.5 eV. The splitting of $2\text{P}_{3/2}$ peak (Fig. 4b) shows the peak at 932.0 eV for Cu^+ which confirmed the presence of Cu^+ in the $\text{CaCu}_3\text{Ti}_4\text{O}_{12}$ lattice. For $\text{CaCu}_3\text{Ti}_4\text{O}_{12}$ /peroxymonosulfate system, the transfer from Cu^+ to Cu^{2+} is irreversible which limits the reaction efficiency. In the visible-light/ $\text{CaCu}_3\text{Ti}_4\text{O}_{12}$ /peroxymonosulfate system, the photo-generated electrons are free to move in the distinct ordered crystallographic sub-lattices reducing Cu^{2+} to Cu^+ and promoting the peroxymonosulfate activation process (Lei et al. 2015). Meanwhile, the photo-generated electrons

can also react with peroxymonosulfate to produce $\text{SO}_4^{\cdot-}$, which enhances the removal of ibuprofen. In addition, Cu^{2+} can also be oxidized into Cu^{3+} by peroxymonosulfate in the $\text{SO}_4^{\cdot-}$ generation process (Liu et al. 2016a, b), and the formed Cu^{3+} has a oxidation potential of 2.3 V in solid form, which can react with water to generate the $\cdot\text{OH}$ (Feng et al. 2016) for the further ibuprofen removal. The peroxymonosulfate performed a dual role in the visible-light/ $\text{CaCu}_3\text{Ti}_4\text{O}_{12}$ /peroxymonosulfate system. First, as an electron acceptor, the peroxymonosulfate molecule reacts with photo-generated electrons to form sulfur radicals thus reducing the rate of electron-hole recombination. Second, as an efficient source of $\text{SO}_4^{\cdot-}$, the peroxymonosulfate molecule is activated with Cu^+ and photo-generated electrons to generate $\text{SO}_4^{\cdot-}$. The CCTO-14 sample after reaction was tested with XPS instrument (Fig. 4a). The test result indicates that the copper in the CCTO-14 sample is stable in the ibuprofen removal process with photo-assistant peroxymonosulfate activation.

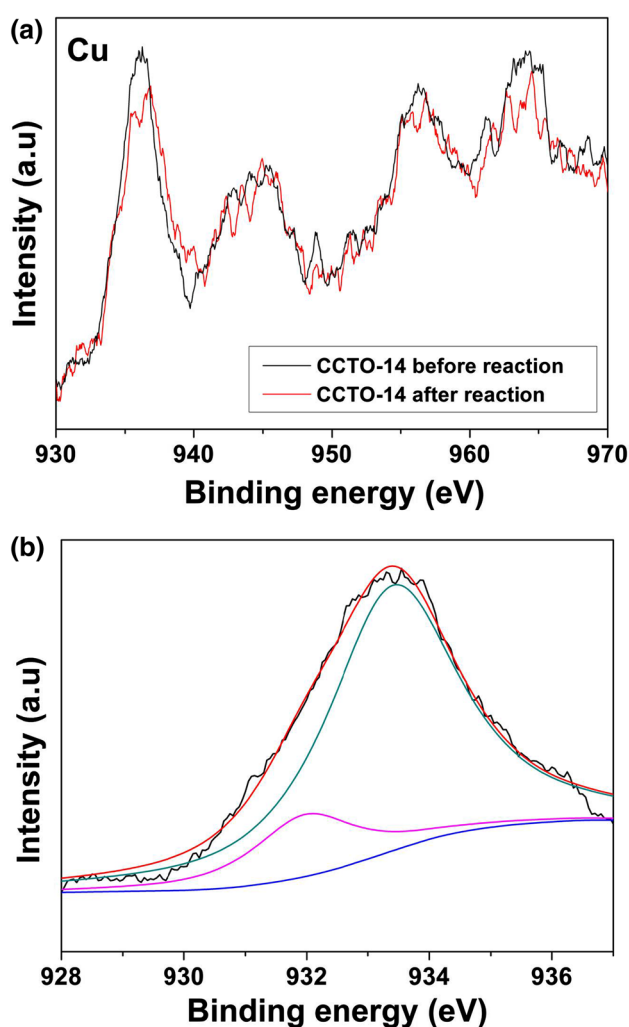


Fig. 4 a X-ray photoelectron spectroscopy (XPS) of CCTO-14 ($\text{CaCu}_3\text{Ti}_4\text{O}_{12}$ sintered at 775 °C for 14 h). The copper was present as copper oxide with $2\text{P}_{3/2}$ peak at 933.6 eV and $2\text{P}_{1/2}$ peak at 953.5 eV. b XPS simulation of $2\text{P}_{3/2}$ peak of copper. The splitting of $2\text{P}_{3/2}$ peak shows the peak at 932.0 eV for Cu^+ which confirmed the presence of Cu^+ in the $\text{CaCu}_3\text{Ti}_4\text{O}_{12}$ lattice

Conclusion

In this study, $\text{CaCu}_3\text{Ti}_4\text{O}_{12}$ crystals were prepared by a molten salt approach from TiO_2 , CuO and CaO mixed with the salts including NaCl and KCl . The catalysts show the morphology of micro-scale cubic and fiber. For ibuprofen removal, the catalysts show higher efficiency in the presence of peroxymonosulfate under visible-light irradiation. The mechanism study shows that the presence of Cu^+ vacancy in the $\text{CaCu}_3\text{Ti}_4\text{O}_{12}$ crystal lattice plays a vital role in activation of peroxymonosulfate. In the ternary visible-light/ $\text{CaCu}_3\text{Ti}_4\text{O}_{12}$ /peroxymonosulfate system, the photo-generated electrons which act as a reductant for Cu^{2+} to Cu^+ promote the peroxymonosulfate activation process dramatically.

Acknowledgements Financial support by the National Nature Science Foundation of China (Grant No. 21507157), the Science and Technology Project of Wenzhou (W20170012), the Startup Foundation for Advanced Talents of Shaanxi University of Science and Technology.

References

- Almeida AFL, Oliveira RS, Goes JC (2002) Structural properties of $\text{CaCu}_3\text{Ti}_4\text{O}_{12}$ obtained by mechanical alloying. *Mater Sci Eng B* 96:275–283. [https://doi.org/10.1016/S0921-5107\(02\)00379-3](https://doi.org/10.1016/S0921-5107(02)00379-3)
- Bu LJ, Shi Z, Zhou SQ (2016) Modeling of Fe(II)-activated persulfate oxidation using atrazine as a target contaminant. *Sep Purif Technol* 169:59–65. <https://doi.org/10.1016/j.sepur.2016.05.037>
- Chen XY, Wang WP, Xiao H (2012) Accelerated TiO_2 photocatalytic degradation of Acid Orange 7 under visible light mediated by peroxymonosulfate. *Chem Eng J* 193–194:290–295. <https://doi.org/10.1016/j.cej.2012.04.033>
- Clark JH, Dyer MS, Palgrave RG (2011) Visible light photo-oxidation of model pollutants using $\text{CaCu}_3\text{Ti}_4\text{O}_{12}$: an experimental

- and theoretical study of optical properties, electronic structure, and selectivity. *J Am Chem Soc* 133:1016–1032. <https://doi.org/10.1021/ja1090832>
- Ding YB, Tang HB, Zhang SH (2016) Efficient degradation of carbamazepine by easily recyclable microscaled CuFeO₂ mediated heterogeneous activation of peroxymonosulfate. *J Hazard Mater* 317:686–694. <https://doi.org/10.1016/j.jhazmat.2016.06.004>
- Duan L, Sun BZ, Wei MY (2015) Catalytic degradation of Acid Orange 7 by manganese oxide octahedral molecular sieves with peroxymonosulfate under visible light irradiation. *J Hazard Mater* 285:356–365. <https://doi.org/10.1016/j.jhazmat.2014.12.015>
- Fang J, Li J, Gao L (2017) Synthesis of OMS-2/graphite nanocomposites with enhanced activity for pollutants degradation in the presence of peroxymonosulfate. *J Colloid Interf Sci* 494:185–193. <https://doi.org/10.1016/j.jcis.2017.01.049>
- Feng Y, Wu DL, Deng Y (2016) Sulfate radical-mediated degradation of sulfadiazine by CuFeO₂ rhombohedral crystal-catalyzed peroxymonosulfate: synergistic effects and mechanisms. *Environ Sci Technol* 50:3119–3127. <https://doi.org/10.1021/acs.est.5b05974>
- Fernandez J, Maruthamuthu P, Kiwi J (2004) Photobleaching and mineralization of orange II by oxone and metal-ions involving Fenton-like chemistry under visible light. *J Photochem Photobiol A* 161:185–192. [https://doi.org/10.1016/S1010-6030\(03\)00293](https://doi.org/10.1016/S1010-6030(03)00293)
- Ghanbaria F, Moradib M, Gohari F (2016) Degradation of 2,4,6-trichlorophenol in aqueous solutions using peroxymonosulfate/activated carbon/UV process via sulfate and hydroxyl radicals. *J Water Process Eng* 9:22–28. <https://doi.org/10.1016/j.jwpe.2015.11.011>
- Gong F, Wang L, Li DW (2015) An effective heterogeneous iron-based catalyst to activate peroxymonosulfate for organic contaminants removal. *Chem Eng J* 267:102–110. <https://doi.org/10.1016/j.cej.2015.01.010>
- Huang JY, Li XF, Ma MJ (2017) Removal of di-(2-ethylhexyl) phthalate from aqueous solution by UV/peroxymonosulfate: influencing factors and reaction pathways. *Chem Eng J* 314:182–191. <https://doi.org/10.1016/j.cej.2016.12.095>
- Jaafarzadeh N, Ghanbari F, Ahmadi M (2017) Efficient integrated processes for pulp and paper wastewater treatment and phytotoxicity reduction: permanganate, electro-Fenton and Co₃O₄/UV/peroxymonosulfate. *Chem Eng J* 308:142–150. <https://doi.org/10.1016/j.cej.2016.09.015>
- Jiang XW, Lia J, Fang J (2017) The photocatalytic performance of g-C₃N₄ from melamine hydrochloride for dyes degradation with peroxymonosulfate. *J Photochem Photobiol A* 336:54–62. <https://doi.org/10.1016/j.jphotochem.2016.12.018>
- Khan S, Han CS, Khan HM (2017) Efficient degradation of lindane by visible and simulated solar light-assisted S-TiO₂/peroxymonosulfate process: kinetics and mechanistic investigations. *J Mol Catal A* 428:9–16. <https://doi.org/10.1016/j.molcata.2016.11.035>
- Kushwaha HS, Madhar NA, Ilahi B (2016) Efficient solar energy conversion using CaCu₃Ti₄O₁₂ photoanode for photocatalysis and photoelectrocatalysis. *Sci Rep* 6:18557. <https://doi.org/10.1038/srep18557>
- Lei Y, Chen CS, Tu YJ (2015) Heterogeneous degradation of organic pollutants by persulfate activated by CuO-Fe₃O₄: mechanism, stability, and effects of pH and bicarbonate ions. *Environ Sci Technol* 49:6838–6845. <https://doi.org/10.1021/acs.est.5b00623>
- Lian LS, Yao B, Hou SD (2017) Kinetic study of hydroxyl and sulfate radical-mediated oxidation of pharmaceuticals in wastewater effluents. *Environ Sci Technol* 51:2954–2962. <https://doi.org/10.1021/acs.est.6b05536>
- Liu Y, Guo HG, Zhang YL (2016a) Activation of peroxymonosulfate by BiVO₄ under visible light for degradation of Rhodamine B. *Chem Phys Lett* 653:101–107. <https://doi.org/10.1016/j.cplett.2016.04.069>
- Liu HZ, Bruton TA, Li W (2016b) Oxidation of benzene by persulfate in the presence of Fe(III)- and Mn(IV)-containing oxides: stoichiometric efficiency and transformation products. *Environ Sci Technol* 50:890–898. <https://doi.org/10.1021/acs.est.5b04815>
- Luo XJ, Liu YS, Yang CP (2015) Oxygen vacancy related defect dipoles in CaCu₃Ti₄O₁₂: detected by electron paramagnetic resonance spectroscopy. *J Eur Ceram Soc* 35:2073–2081. <https://doi.org/10.1016/j.jeurceramsoc.2015.01.024>
- Luo L, Wu D, Dai D (2017) Synergistic effects of persistent free radicals and visible radiation on peroxymonosulfate activation by ferric citrate for the decomposition of organic contaminants. *Appl Catal B* 205:404–411. <https://doi.org/10.1016/j.apcatb.2016.12.060>
- Ponce MA, Ramirez MA, Schipani F (2015) Electrical behavior analysis of n-type CaCu₃Ti₄O₁₂ thick films exposed to different atmospheres. *J Eur Ceram Soc* 35:153–161. <https://doi.org/10.1016/j.jeurceramsoc.2014.08.041>
- Ramirez AP, Subramanian MA, Gar M (2000) Giant dielectric constant response in a copper-titanate. *Solid State Commun* 115:217–220. [https://doi.org/10.1016/S0038-1098\(00\)00182-4](https://doi.org/10.1016/S0038-1098(00)00182-4)
- Vivas L, Delgado GE, Leret P (2017) Electron paramagnetic resonance study of hopping in CCTO mixed with TiO₂. *J Alloy Compd* 692:212–218. <https://doi.org/10.1016/j.jallcom.2016.09.034>
- Wang YX, Zhou L, Duan XG (2015) Photochemical degradation of phenol solutions on Co₃O₄ nanorods with sulfate radicals. *Catal Today* 258:576–584. <https://doi.org/10.1016/j.cattod.2014.12.020>
- Yang QJ, Choi H, Chen YJ (2008) Heterogeneous activation of peroxymonosulfate by supported cobalt catalysts for the degradation of 2,4-dichlorophenol in water: the effect of support, cobalt precursor, and UV radiation. *Appl Catal B* 77:300–307. <https://doi.org/10.1016/j.apcatb.2007.07.020>
- Yi K, Lin A, Zhang ZY (2017) Metal-free activation of oxone using one-step prepared sulfur-doped carbon nitride under visible light irradiation. *Sep Purif Technol* 173:72–79. <https://doi.org/10.1016/j.seppur.2016.09.008>
- Zhang WX, Li LQ, Li P (2016) A novel method to synthesize CaCu₃Ti₄O₁₂ with acetylacetonate precursor. *Mater Lett* 181:71–73. <https://doi.org/10.1016/j.matlet.2016.06.003>
- Zhu Y, Chen S, Quan X (2013) Cobalt-doped TiO₂ nanocatalyst for heterogeneous activation of peroxymonosulfate. *RSC Adv* 3:520–525. <https://doi.org/10.1039/C2RA22039C>
- Zou J, Ma J, Zhang X (2014) Rapid spectrophotometric determination of peroxymonosulfate in water with cobalt-mediated oxidation decolorization of methyl orange. *Chem Eng J* 253:34–39. <https://doi.org/10.1016/j.cej.2014.05.042>